Muñoz-Portero, M.; Nachiondo Farinós, TDM.; Blasco-Tamarit, E.; Vicent-Blesa, A.; Garcia-Anton, J. (10-2). Potential-pH Diagrams of Iron in Concentrated Aqueous LiBr Solutions at 25°C. Corrosion. 74(10):1102-1116. https://doi.org/10.5006/2865

Potential-pH diagrams of iron in concentrated aqueous LiBr solutions at 25 ºC

M.J. Muñoz-Portero,* T. Nachiondo,** E. Blasco-Tamarit,* A. Vicent-Blesa,* J. García-Antón,*'***

Keywords:

Equilibrium (reversible) potential
Oxidation
Passivation
pH changes and effects
Potential-pH diagram
Stainless steels

*Ingeniería Electroquímica y Corrosión (IEC), Instituto Universitario de Investigación de Seguridad Industrial, Radiofísica y Medioambiental, Universitat Politècnica de València, Camino de Vera, s/n, 46022 Valencia (Spain)

**Departamento de Informática de Sistemas y Computadores, Universitat Politècnica de València, Camino de Vera, s/n, 46022 Valencia (Spain)

***Corresponding author: Phone: +34 963877632; Fax: +34 963877639. Email: jgarciaa@iqn.upv.es.

ABSTRACT

Potential-pH diagrams of iron are developed in aqueous LiBr solutions with concentrations of 400 g/L, 700 g/L, 850 g/L, and 992 g/L LiBr at 25 °C, which are common concentrations in different parts of absorption machines. Comparison of the potential-pH diagrams of iron in the absence and the presence of concentrated aqueous LiBr solutions shows that the corrosion area at acid, neutral, and weak alkaline pH extends to lower potentials and higher pH values with the increase of LiBr concentration, as a result of formation of the aqueous species $FeBr_2(aq)$ and $FeBr_3(aq)$ and destabilization of the solid species Fe, $Fe(OH)_2(s)$, Fe_3O_4, and Fe_2O_3.

INTRODUCTION

Nowadays, absorption refrigeration systems can be considered as the alternative to replace the conventional vapor compression refrigerating systems in certain industrial and domestic processes. Aqueous lithium bromide (LiBr) solutions with high concentrations are used widely as absorbents in the absorption machines because they have favorable thermophysical properties.[1-10] However, LiBr solutions are an aggressive medium, which can cause corrosion on metallic materials (copper, titanium, nickel, stainless steel, etc.) in absorption plants.[11-26]

Double and triple effect LiBr absorption machines have been developed with the technological advances, which have higher energetic efficiency than single effect machines.[7-10] Although these machines also reach both higher LiBr concentrations and temperatures, they may present important corrosion problems. The use of inhibitors or the control of pH in the solutions may be a way to reduce corrosion problems.

In absorption machines with LiBr there are different components built with different metallic alloys, all assembled in electrical contact at different concentrations and temperatures. The condenser, the evaporator, and the absorber must be constructed of highly alloyed stainless steels because they have good combination of mechanical properties and corrosion resistance. The chromium content of the stainless steels is the cause of their resistance to corrosion because a film of chromium oxide is formed on its surface protecting the materials.[27-29] When this film disappears the iron present in the stainless steels is oxidized. Knowledge of iron corrosion is therefore an important aspect. Several studies have researched the kinetic of corrosion of stainless steels in highly concentrated LiBr solutions, in which iron is the main component.[11-16,24,25] One way to understand and predict the iron corrosion is to consider the thermodynamic aspects.

The potential-pH (E-pH) diagrams, also known as Pourbaix diagrams, are used to predict and study corrosion processes from the point of view of thermodynamics. They show the thermodynamic regions of immunity (stability of a metal, i.e. no corrosion), passivation (stability of a solid compound), and corrosion (stability of an aqueous compound) for a metal in a specific medium.[30-35] Potential-pH diagrams are constructed by calculation of the equilibrium conditions between metallic compounds using the Nernst equation (for the case of the electrochemical equilibria) and the equilibrium constant (for the case of chemical equilibria).

In previous works potential-pH diagrams of copper,[36] nickel,[37] chromium,[38] and titanium[39] have been developed in aqueous LiBr solutions with high concentrations at 25 °C, which have been used to analyze the corrosion of these metals in absorption machines. The construction of potential-pH diagrams of iron in concentrated aqueous LiBr solutions could be useful to predict and study the corrosion of stainless steels in absorption machines, because iron is the main component.

The aim of this work is the prediction and the analysis of iron corrosion in similar conditions to those existing in LiBr absorption machines. For this purpose, potential-pH diagrams of iron in aqueous LiBr solutions with concentrations of 400 g/L, 700 g/L, 850 g/L, and 992 g/L at 25 °C are constructed and they are compared with the potential-pH diagram of iron in water (H_2O) at 25 °C.

PROCEDURE

Methodology followed for the construction of the potential-pH diagrams of iron in concentrated aqueous LiBr solutions is similar to that used for other metals in the same LiBr conditions.[36-39] In this work, it has been particularized for the case of iron.

Chemical species

The ternary $Fe\text{-}Br^{-}\text{-}H_2O$ system is considered for the construction of the potential-pH diagrams of iron in concentrated aqueous LiBr solutions. It is considered a total number of twenty-two chemical species: fourteen aqueous and eight solid species.

- Aqueous species: Fe^{+2}, $FeOH^{+}$, $Fe(OH)_2(aq)$, $Fe(OH)_3^{-}$, $Fe(OH)_4^{-2}$, Fe^{+3}, $FeOH^{+2}$, $Fe(OH)_2^{+}$, $Fe(OH)_3(aq)$, $Fe(OH)_4^{-}$, FeO_4^{-2}, $FeBr_2(aq)$, $FeBr^{+2}$, and $FeBr_3(aq)$.
- Solid species: Fe, $Fe(OH)_2(s)$, $\alpha\text{-}Fe_3O_4$, $Fe(OH)_3(s)$, α-FeOOH, $\alpha\text{-}Fe_2O_3$, $FeBr_2(s)$, and $FeBr_3(s)$.

For the construction of the potential-pH diagram of iron in H_2O only seventeen chemical species are considered (Fe-H_2O system).

Table 1 shows all the species containing iron used for the construction of the potential-pH diagrams. It also is indicated the oxidation number, the state of the species, the standard Gibbs free energy of formation ($\Delta G_f°$) data at 25 °C, and the reference of the data.[40-42] These $\Delta G_f°$ data could be used to calculate the equilibrium conditions.

Reactions

Reactions are determined considering pairs of species containing iron, according to the Equation (1):

$$xY + mH^+ + ne^- \rightleftarrows yY + aH_2O + bBr^- \quad (1)$$

where X and Y are the pair of species containing iron in the reaction. In each reaction it also can be considered the hydrogen ion (H^+), the electrical charge (e^-), the H_2O, and the bromide ion (Br^-).

Tables 2-5 show the equations of the different reactions used for the Fe-Br^--H_2O system. It is considered a total number of 231 reactions, which are classified into four types:

- Electrochemical reactions not involving H^+, with 27 reactions (Table 2).
- Electrochemical reactions involving H^+, with 121 reactions (Table 3).
- Chemical reactions involving H^+, with 67 reactions (Table 4).
- Chemical reactions not involving H^+, with 16 reactions (Table 5).

These reactions are divided into three subtypes: 1) homogeneous (considering only aqueous species), 2) heterogeneous with two solid species, and 3) heterogeneous with one solid species.

Equilibrium conditions

For the Fe-Br^--H_2O system the equilibrium conditions are calculated from $\Delta G_f°$ data at 25 °C following conventional procedures.[30]

Previously it is necessary to determine the Br^- ion activity and the H_2O activity representative of the tested aqueous LiBr solutions. The calculation of the activity values is realized using the method proposed by Meissner and Kusik.[43-45] For the aqueous LiBr solutions with concentrations of 400 g/L, 700 g/L, 850 g/L, and 992 g/L at 25 °C, the calculated values are 15.61, 194.77, 650.06, and 2,042.65 for the Br^- ion activity and 0.715, 0.358, 0.216, and 0.118 for the H_2O activity, respectively, as it has been indicated in previous works.[36-39]

The thermodynamic method of Meissner and Kusik is verified using vapor pressure and mean activity coefficient data for LiBr-based systems. The water activity in aqueous LiBr solution can be expressed as the ratio of the water vapor pressures over the LiBr solution and over pure water ($p/p_w°$). Figure 1 shows results of vapor pressure calculations for the LiBr+H_2O solution as a function of LiBr molality at 25 °C. It is obtained very good agreement with the literature data proposed by Pennington.[46,47] Similarly, Figure 2 shows the mean activity coefficient calculations for the LiBr+H_2O solution as a function of LiBr molality at 25 °C. The calculated values are compared with the literature data.[41] The agreement with literature data of vapor pressure and mean activity coefficient data indicates that the method proposed by Meissner and Kusik correctly reproduces activities of solution species. Thus, activities can be used with confidence in the calculation of the equilibrium conditions.

All the electrochemical and chemical equilibria are calculated using a new software developed in a previous work.[48]

Three types of diagrams are constructed: 1) predominance diagrams of the aqueous iron species (showing only the stable aqueous species containing iron), 2) potential-pH diagrams of iron (showing all the stable species containing iron), and 3) simplified potential-pH diagrams of iron (showing only the areas of corrosion, alkaline corrosion, immunity, and passivation).

All diagrams are drawn using Autocad software.

RESULTS

Figures 3-7 show the predominance diagrams of the aqueous iron species at 25 °C in the absence (Figure 3) and in the presence of LiBr solutions with concentrations of 400 g/L (Figure 4), 700 g/L (Figure 5), 850 g/L (Figure 6), and 992 g/L (Figure 7). Only equilibria between aqueous species involving iron are shown in the lines on the diagrams.

Figures 8-12 show the potential-pH diagrams of iron in H_2O at 25 °C in the absence (Figure 8) and in the presence of LiBr solutions with concentrations of 400 g/L (Figure 9), 700 g/L (Figure 10), 850 g/L (Figure 11), and 992 g/L (Figure 12). Equilibria between aqueous and/or solid species involving iron are shown in the lines on the diagrams. All the diagrams are constructed considering activity values of the aqueous iron species of 10^{-6}, 10^{-4}, 10^{-2}, and 10^{0}.

Table 6 shows the thermodynamic stability of the species containing iron for the Fe-Br^--H_2O system in concentrated aqueous LiBr solutions at 25 °C. Marked species in Table 6 appear in the diagrams shown in Figures 1-10 at some LiBr concentration.

Figure 13 shows the simplified potential-pH diagrams of iron in H_2O at 25 °C in the absence (Figure 13a) and in the presence of 400 g/L (Figure 13b), 700 g/L (Figure 13c), 850 g/L (Figure 13d), and 992 g/L (Figure 13e) LiBr solutions. All the diagrams in Figure 13 are constructed considering an activity value of the aqueous iron species of 10^{-6}. The stability regions of the iron species are not shown in the simplified potential-pH diagrams, and they only show the areas of corrosion, alkaline corrosion, immunity, and passivation. The corrosion and alkaline corrosion areas are shaded to differentiate them from immunity and passivation areas.

In Figures 3-13 there are two broken lines, “a” and “b”, which delimit the stability region of H_2O at a partial pressure of the gaseous species equal to 1 atm. Line “a” shows the equilibrium between H_2O and oxygen and line “b” shows the equilibrium between H_2O and hydrogen.

The potential values reported in this work are always related to the standard hydrogen electrode (SHE), which is considered to be zero at 25 °C.

The potential-pH diagrams of iron in aqueous LiBr solutions with concentrations of 400 g/L, 700 g/L, 850 g/L, and 992 g/L at 25 °C are original in this work and they have not been reported in the literature.

DISCUSSION

Predominance diagrams of the aqueous iron species in concentrated aqueous LiBr solutions

Predominance diagram of the aqueous iron species at 25 °C (Figure 3) shows the stability area of aqueous iron species, considering oxidation numbers II, III, and VI. The stable iron species with oxidation number II are Fe^{+2}, $FeOH^{+}$, $Fe(OH)_2$(aq), $Fe(OH)_3^{-}$, and $Fe(OH)_4^{-2}$. The stable iron species with oxidation number III are Fe^{+3}, $FeOH^{+2}$, $Fe(OH)_2^{+}$, $Fe(OH)_3$(aq), and $Fe(OH)_4^{-}$. Finally, the only stable iron species with oxidation number VI is FeO_4^{-2}.

Predominance diagrams of the aqueous iron species in LiBr solutions with concentrations of 400 g/L, 700 g/L, 850 g/L, and 992 g/L at 25 °C (Figures 4-7, respectively) show that Fe^{+2} is not stable and $FeBr_2$(aq) is the stable aqueous iron species with oxidation number II at acid pH, whose stability area extends to neutral and weak alkaline pH. For oxidation number III, Fe^{+3} is not stable and $FeBr_3$(aq) is the stable aqueous iron species at acid pH.

Equation (2) shows the chemical reaction not involving H^{+} between Fe^{+2} and $FeBr_2$(aq). Equation (3) shows the equilibrium constant (K) at 25 °C for this reaction:

$$Fe^{+2} + 2Br^{-} \rightleftarrows FeBr_2(aq) \qquad (2)$$

$$K = \left[\frac{(FeBr_2(aq))}{(Fe^{+2})(Br^{-})^2}\right] = 5.2430\cdot10^{-3} \qquad (3)$$

Aqueous $FeBr_2$(aq) is formed at a Br^{-} ion activity higher than 13.81, which is happening in all the aqueous LiBr solutions studied in this work. Therefore, $FeBr_2$(aq) is the stable species.

The increase in the LiBr concentration (i.e. the increase in the Br^{-} ion activity and the decrease in the H_2O activity) from 400 g/L to 992 g/L extends the predominance area of $FeBr_2$(aq) to higher pH. This is due to the destabilization of aqueous $FeOH^{+}$, which is not stable for LiBr concentrations of 700 g/L, 850 g/L, and 992 g/L, as shown in Figures 5-7, respectively.

Equation (4) shows the chemical reaction not involving H^{+} between Fe^{+3} and $FeBr_3$(aq). Equation (5) shows the equilibrium constant (K) at 25 °C for this reaction:

$$Fe^{+3} + 3Br^{-} \rightleftarrows FeBr_3(aq) \qquad (4)$$

$$K = \left[\frac{(FeBr_3(aq))}{(Fe^{+3})(Br^{-})^3}\right] = 5.7068\cdot10^{-3} \qquad (5)$$

Aqueous $FeBr_3$(aq) is formed at a Br^{-} ion activity higher than 5.60. For all the aqueous LiBr solutions studied, Br^{-} ion activity is higher than this value and therefore, $FeBr_3$(aq) is the stable species.

The predominance area of $FeBr_3$(aq) extends to higher pH with increasing LiBr concentration from 400 g/L to 992 g/L, as a result of destabilization of $FeOH^{+2}$ and $Fe(OH)_2^{+}$ species. $FeOH^{+2}$ is not stable for all the LiBr concentrations studied and $Fe(OH)_2^{+}$ is not stable for a LiBr concentration of 992 g/L, as shown in Figure 7.

Potential-pH diagrams of iron in concentrated aqueous LiBr solutions

Potential-pH diagram of iron in H_2O at 25 °C (Figure 8) shows that the stability area of iron (i.e. immunity area) is situated below the broken line "b", which correspond to the equilibrium between H_2O and hydrogen. It significates that iron is a very reactive metal.

Iron can oxidize to form iron species with oxidation number II: aqueous Fe^{+2}, solid $Fe(OH)_2$(s), and aqueous $Fe(OH)_4^{-2}$. For an activity value of the aqueous iron species of 10^{-6}, aqueous Fe^{+2} forms a corrosion area at acid, neutral, and weak alkaline pH, solid $Fe(OH)_2$(s) forms a passivation area at alkaline pH, and aqueous $Fe(OH)_4^{-2}$ forms an alkaline corrosion area at very strong alkaline pH. Electrochemical equilibrium potential between iron and Fe^{+2} shifts to a higher value with an increase in the Fe^{+2} activity from 10^{-6} to 10^{0}, decreasing the corrosion area of Fe^{+2} and increasing the immunity area of the iron. Electrochemical equilibrium between iron and $Fe(OH)_4^{-2}$ shifts to both higher pH values and potentials with the increase in the $Fe(OH)_4^{-2}$ activity, decreasing the alkaline corrosion area of $Fe(OH)_4^{-2}$ and increasing the immunity area of the iron. Finally, the size of the passivation area of $Fe(OH)_2$(s) increases with an increase in the activity of the aqueous iron species from 10^{-6} to 10^{0}, because it results in a lower pH value for the chemical equilibrium between Fe^{+2} and $Fe(OH)_2$(s) and a higher pH value for the chemical equilibrium between $Fe(OH)_2$(s) and $Fe(OH)_4^{-2}$. Consequently, the corrosion area of Fe^{+2} and the alkaline corrosion area of $Fe(OH)_4^{-2}$ decrease with the increase in the activity of the aqueous iron species.

For alkaline solutions, Fe (II) species (Fe^{+2}, $Fe(OH)_2$(s) and $Fe(OH)_4^{-2}$) can oxidize to form the solid compound Fe_3O_4, with oxidation number II/III ($Fe^{+2}(Fe^{+3})_2O_4$).

Aqueous Fe (II) species (Fe^{+2} and $Fe(OH)_4^{-2}$) and the solid compound Fe_3O_4 can oxidize to form the iron species with oxidation number III: aqueous Fe^{+3}, solid Fe_2O_3, and aqueous $Fe(OH)_4^{-}$. Considering an activity value of the aqueous iron species of 10^{-6}, aqueous Fe^{+3} forms a corrosion area at acid pH, solid Fe_2O_3 forms a wide passivation area, and aqueous $Fe(OH)_4^{-}$ forms an alkaline corrosion area at very strong alkaline pH. An increase in the activity value of the aqueous iron species from 10^{-6} to 10^{0} results in a decrease of the pH for the chemical equilibrium between Fe^{+3} and Fe_2O_3, and an increase of the pH for the chemical equilibrium between Fe_2O_3 and $Fe(OH)_4^{-}$. Consequently, the size of the passivation area of Fe_2O_3 increases with the increase in the activity of the aqueous iron species, decreasing the corrosion area of Fe^{+3} and the alkaline corrosion area of $Fe(OH)_4^{-}$.

Fe (III) species (aqueous Fe^{+3}, solid Fe_2O_3, and aqueous $Fe(OH)_4^{-}$) can oxidize to form aqueous FeO_4^{-2} species with oxidation number VI, which creates a corrosion area at high potentials. The equilibrium between Fe_2O_3 and FeO_4^{-2} shifts to both higher pH values and potentials with an increase in the FeO_4^{-2} activity from 10^{-6} to 10^{0}. Consequently, the size of the corrosion area of FeO_4^{-2} at high potentials decreases with the increase in the activity of the aqueous iron species, increasing the passivation area of Fe_2O_3.

Comparison of the potential-pH diagram of iron in H_2O at 25 °C in Figure 8 with the potential-pH diagrams of iron in aqueous LiBr solutions with concentrations of 400 g/L, 700 g/L, 850 g/L, and 992 g/L at 25 °C (Figures 9-12, respectively) shows that the corrosion area at acid, neutral, and weak alkaline pH extends to lower potentials and higher pH values with increasing LiBr concentration (i.e. increasing Br^{-} activity and decreasing H_2O activity), as a result of formation of the aqueous species $FeBr_2$(aq) and $FeBr_3$(aq) and destabilization of the solid species Fe, $Fe(OH)_2$(s), Fe_3O_4, and Fe_2O_3.

Equation (6) shows the electrochemical reaction not involving H^{+} between Fe and aqueous $FeBr_2$(aq), with the equilibrium potential given by corresponding Nernst equation at 25 °C, as shown in Equation (7):

$$FeBr_2(aq) + 2e^{-} \rightleftarrows \mathbf{Fe} + 2Br^{-} \qquad (6)$$

$$E_{FeBr_2(aq)/\mathbf{Fe}}\,(V_{SHE}) = -\,0.409\; +$$

$$0.0296\ \log\left[\frac{(FeBr_2(aq))}{(Br^-)^2}\right] \qquad (7)$$

Considering an activity value of the aqueous iron species of 10^{-6}, Fe corrodes to form aqueous $FeBr_2(aq)$ at a potential value higher than – 0.657 V_{SHE}, – 0.722 V_{SHE}, – 0.752 V_{SHE}, and – 0.782 V_{SHE} in aqueous LiBr solutions with concentrations of 400 g/L, 700 g/L, 850 g/L, and 992 g/L, respectively, as shown in Figures 9-12. For each LiBr concentration, an increase in aqueous $FeBr_2(aq)$ activity from 10^{-6} to 10^{0} results in an increase of potential value for the equilibrium between Fe and aqueous $FeBr_2(aq)$. In the absence of aqueous LiBr solutions, Fe corrodes to form aqueous Fe^{+2} at a potential higher than – 0.654 V_{SHE} for aqueous Fe^{+2} activity of 10^{-6}, as shown in Figure 8.

Equation (8) shows the chemical reaction involving H^+ between aqueous $FeBr_2(aq)$ and solid $Fe(OH)_2(s)$. Equation (9) shows the equilibrium pH at 25 °C for this reaction:

$$FeBr_2(aq)\; +\; 2H_2O\; \overset{\rightarrow}{\leftarrow}\; \mathbf{Fe(OH)_2(s)}\; +$$

$$2Br^-\; +\; 2H^+ \qquad (8)$$

$$pH = \frac{2\log(Br^-) - \log(FeBr_2(aq)) -}{2}$$

$$\frac{2\log(H_2O) + 10.735}{2} \qquad (9)$$

Considering an activity value of the aqueous iron species of 10^{-6}, the formation of solid $Fe(OH)_2(s)$ from aqueous $FeBr_2(aq)$ occurs at a pH value higher than 9.71 in aqueous LiBr solutions with concentration of 400 g/L, as shown in Figure 9. An increase in aqueous $FeBr_2(aq)$ activity from 10^{-6} to 10^{0} results in a decrease of the pH value for the chemical equilibrium between aqueous $FeBr_2(aq)$ and solid $Fe(OH)_2(s)$. For aqueous LiBr solutions with concentrations of 700 g/L, 850 g/L, and 992 g/L, $Fe(OH)_2(s)$ is not stable, as shown in Figures 10-12. In the absence of aqueous LiBr solutions, $Fe(OH)_2(s)$ is formed from Fe^{+2} at a pH value higher than 9.51 for aqueous Fe^{+2} activity of 10^{-6} and a water activity of 1, as shown in Figure 8.

Equation (10) shows the electrochemical reaction involving H^+ between aqueous $FeBr_2(aq)$ and solid Fe_3O_4, with the equilibrium potential given by Nernst equation at 25 °C, as shown Equation (11):

$$\mathbf{Fe_3O_4}\; +\; 6Br^-\; +\; 8H^+\; +$$

$$2e^-\; \overset{\rightarrow}{\leftarrow}\; 3FeBr_2(aq)\; +\; 4H_2O \qquad (10)$$

$$E_{\mathbf{Fe_3O_4}/FeBr_2(aq)}\,(V_{SHE}) = 0.895\; +$$

$$0.0296\ \log\left[\frac{(Br^-)^6}{(FeBr_2(aq))^3\,(H_2O)^4}\right] - 0.237\ pH \qquad (11)$$

For each value of the aqueous $FeBr_2(aq)$ activity, the electrochemical equilibrium between aqueous $FeBr_2(aq)$ and solid Fe_3O_4 shifts to both higher potentials and pH values with the increase of LiBr concentration, as shown in Figures 9-12. In the absence of aqueous LiBr solution, solid Fe_3O_4 is formed from aqueous Fe^{+2}, as shown in Figure 8.

Solid Fe_2O_3 can be formed from aqueous $FeBr_2(aq)$ or $FeBr_3(aq)$. Equation (12) shows the electrochemical reaction involving H^+ between aqueous $FeBr_2(aq)$ and solid Fe_2O_3, with the equilibrium potential given by Nernst equation at 25 °C, as shown in Equation (13):

$$\mathbf{Fe_2O_3}\; +\; 4Br^-\; +\; 6H^+\; +\; 2e^-\; \overset{\rightarrow}{\leftarrow}$$

$$2FeBr_2(aq)\; +\; 3H_2O \qquad (12)$$

$$E_{\mathbf{Fe_2O_3}/FeBr_2(aq)}\,(V_{SHE}) = 0.648\; +$$

$$0.0296\ \log\left[\frac{(Br^-)^4}{(FeBr_2(aq))^2\,(H_2O)^3}\right] - 0.177\ pH \qquad (13)$$

For each value of the aqueous $FeBr_2(aq)$ activity, the electrochemical equilibrium between aqueous $FeBr_2(aq)$ and solid Fe_2O_3 shifts at both higher potentials and pH values when the LiBr concentration increases, as shown in Figures 9-12. In the absence of aqueous LiBr solutions, Fe_2O_3 is formed from aqueous Fe^{+2}, as shown in Figure 8.

Equation (14) shows the chemical reaction involving H^+ between aqueous $FeBr_3(aq)$ and solid Fe_2O_3. Equation (15) shows the equilibrium pH at 25 °C for this reaction:

$$2FeBr_3(aq)\; +\; 3H_2O\; \overset{\rightarrow}{\leftarrow}\; \mathbf{Fe_2O_3}\; +$$

$$6Br^-\; +\; 6H^+ \qquad (14)$$

$$pH = \frac{6\log(Br^-) - 2\log(FeBr_3(aq)) -}{6}$$

$$\frac{3\log(H_2O) - 4.064}{6} \qquad (15)$$

For an aqueous $FeBr_3(aq)$ activity of 10^{-6}, the formation of solid Fe_2O_3 from aqueous $FeBr_3(aq)$ occurs at a pH value higher than 2.59, 3.84, 4.47, and 5.10 in aqueous LiBr solutions with concentrations of 400 g/L, 700 g/L, 850 g/L, and 992 g/L, respectively, as shown in Figures 9-12. An increase in aqueous $FeBr_3(aq)$ activity from 10^{-6} to 10^{0} results in a decrease of the pH value for the chemical equilibrium between aqueous $FeBr_3(aq)$ and solid Fe_2O_3. In the absence of aqueous LiBr solutions, Fe_2O_3 is formed from aqueous Fe^{+3}, as shown in Figure 8.

The alkaline corrosion area due to the aqueous species $Fe(OH)_4^{-2}$ and $Fe(OH)_4^{-}$ at very strong alkaline pH shifts to both higher potentials and pH values with the increase of LiBr concentration from 400 g/L to 992 g/L, as shown in Figures 9-12. The aqueous $Fe(OH)_4^{-}$ species only appears in the potential-pH diagram of iron in aqueous LiBr solutions with concentration of 400 g/L, considering an aqueous $Fe(OH)_4^{-}$ activity of 10^{-6} (Figure 9) and it disappears in the potential-pH diagrams of iron in aqueous LiBr solutions with concentrations of 700 g/L, 850 g/L, and 992 g/L (Figures 10-12).

The stable Fe (III) species in the presence of aqueous LiBr solutions with concentrations of 400 g/L, 700 g/L, 850 g/L, and 992 g/L are aqueous $FeBr_3$(aq), solid Fe_2O_3, and aqueous $Fe(OH)_4^-$). These species can oxidize to form aqueous FeO_4^{-2}, which creates a corrosion area at high potentials. The oxidation of aqueous $FeBr_3$(aq) or solid Fe_2O_3 to form aqueous FeO_4^{-2} occurs at both higher potentials and pH values with increasing LiBr concentration from 400 g/L to 992 g/L, as shown in Figures 9-12. The oxidation of aqueous $Fe(OH)_4^-$ to form aqueous FeO_4^{-2} is independent of the H_2O activity and therefore, it not depends on the LiBr concentration. Consequently, the size of the corrosion area at high potentials decreases slightly with increasing LiBr concentration.

Simplified potential-pH diagrams of iron in concentrated aqueous LiBr solutions

Figure 13 shows the effect of LiBr concentration on the simplified potential-pH diagrams of iron in H_2O at 25 °C. It is observed that the corrosion area at acid, neutral, and weak alkaline pH shifts to lower potentials and higher pH values with the increase of LiBr concentration. The corrosion area at high potentials decreases slightly with the increase of LiBr concentration. The alkaline corrosion area shifts to both higher potentials and higher pH values with increasing LiBr concentration. On the other hand, the immunity and the passivation areas decrease with increasing LiBr concentration.

Potential-pH diagrams of iron in aqueous LiBr solutions with concentration of 400 g/L, 700 g/L, 850 g/L, and 992 g/L at 25 °C, showing the areas of corrosion, alkaline corrosion, immunity, and passivation, could be an useful tool to better understand the corrosion behaviour of stainless steels in absorption machines, in which the iron is the main component.[11-16,24,25]

CONCLUSIONS

Potential-pH diagrams of iron have been developed in aqueous LiBr solutions with concentrations of 400 g/L, 700 g/L, 850 g/L, and 992 g/L at 25 °C, in similar conditions to those existing in the LiBr absorption machines. These diagrams could be an useful tool to predict and study the corrosion behavior of stainless steels in absorption machines, in which the iron is the main component. Comparison of the potential-pH diagrams of iron in the absence and the presence of concentrated aqueous LiBr solutions indicates that:

- The corrosion area at acid, neutral, and weak alkaline pH extends to lower potentials and higher pH values with the increase of LiBr concentration, as a result of formation of the aqueous species $FeBr_2$(aq) and $FeBr_3$(aq) and destabilization of the solid species Fe, $Fe(OH)_2$(s), Fe_3O_4, and Fe_2O_3.

- The alkaline corrosion area due to the aqueous species $Fe(OH)_4^{-2}$ and $Fe(OH)_4^-$ at very strong alkaline pH shifts to both higher potentials and higher pH values with increasing LiBr concentration.

- The corrosion area at high potentials due to the aqueous species FeO_4^{-2} decreases slightly with increasing LiBr concentration.

- An increase in the LiBr concentration results in a decrease of the immunity area of the iron and the passivation area due to the solid species $Fe(OH)_2$(s), Fe_3O_4, and Fe_2O_3.

ACKNOWLEDGEMENTS

The authors acknowledge to “Programa de Apoyo a la Investigación y Desarrollo (PAID-06-10) de la UPV” for the support of this work, Antonio Juncos for his assistance in plotting the diagrams, and Dra. M. Asunción Jaime for her translation assistance.

REFERENCES

1. J.W. Furlong, *The Air Pollution Consultant* 11/12 (1994): p. 1.12-1.14.
2. A.D. Althouse, C.H. Turnquist, A.F. Bracciano, *Modern Refrigeration and Air Conditioning,* 18th ed. (Illinois: Goodheart-Willcox, 2004).
3. S-F. Lee, S.A. Sherif, *ASHRAE Trans.* 105 (1999): p. 1256-1266.
4. F.A. Holland, *Appl. Therm. Eng.* 20 (2000): p. 863-871.
5. J. Siqueiros, R.J. Romero, *Appl. Therm. Eng.* 27 (2007): p. 1043-1053.
6. R.J. Romero, J. Siqueiros, A. Huicochea, *Appl. Therm. Eng.* 27 (2007): p. 1054-1061.
7. G. Shu, J. Che, H. Tian, X. Wang, P. Liu, *Appl. Therm. Eng.* 112 (2017): p. 1626-1637.
8. R. Maryami, A.A. Dehghan, *Appl. Therm. Eng.* 124 (2017): p. 103-123.
9. M. Yang, S.Y. Lee, J.T. Chung, Y.T. Kang, *Appl. Energy* 187 (2017): p. 243-254.
10. W. Rivera, A. Huicochea, R.J. Romero, A. Lozano, *Appl. Therm. Eng.* 132 (2018): p. 432-440.
11. R. Leiva-García, M.J. Muñoz-Portero, J. García-Antón, *Corros. Sci.* 52 (2010): p. 950-959.
12. R. M. Fernández-Domene, E. Blasco-Tamarit, D.M. García-García, J. García-Antón, *Corros. Sci.* 52 (2010): p. 3453-3464.
13. E. Blasco-Tamarit, D.M. García-García, J. García-Antón, *Corros. Sci.* 53 (2011): p. 784-795.
14. R. Sánchez-Tovar, M.T. Montañés, J. García-Antón, *Corros. Sci.* 53 (2011): p. 2598-2610.
15. R. Leiva-García, M.J. Muñoz-Portero, J. García-Antón, *Int. J. Electrochem. Sci.* 6 (2011): p. 442-460.
16. R.M. Fernández-Domene, E. Blasco-Tamarit, D.M. García-García, J. García-Antón, *Corros. Sci.* 55 (2012): p. 40-53.
17. R. Sánchez-Tovar, M.T. Montañés, J. García-Antón, *Corros. Sci.* 60 (2012): p. 118-128.
18. M.T. Montañés, R. Sánchez-Tovar, J. García-Antón, V. Pérez-Herranz, *Corrosion* 68 (2012): p. 411-420.
19. R. Sánchez-Tovar, M.T. Montañés, J. García-Antón, *Corros. Sci.* 68 (2013): p. 91-100.
20. R. Sánchez-Tovar, M.T. Montañés, J. García-Antón, *Corros. Sci.* 73 (2013): p. 365-374.
21. A.E. El Meleigy, S.E. Abd Elhamid, A.A. El Warraky, *Materwiss Werksttech* 46 (2015): p. 59-68.
22. A. Soliz, L. Caceres, *Int. J. Electrochem. Sci.* 10 (2015): p. 5673-5693.
23. J. Li, C. Liang, N. Huang, *J. Mater. Eng. Perform.* 24 (2015): p. 4456-4461.
24. E.A. Abd El Meguid, S.S. Abd El Rehim, S.A. Al Kiey, *Corros. Eng. Sci. Techn.* 51 (2016): p. 429-437.
25. A. Goodarzi, I. Danaee, H. Eskandari, S. Nikmanesh, *J. Electrochem. Sci. Technol.* 7 (2016): p. 58-67.
26. X. Zhao, C. Lin, Y. Yang, Y. Zhang, *Rare Metal Mat. Eng.* 46 (2017): p. 3935-3940.
27. Y.F. Cheng, J.L. Luo, *Electrochim. Acta* 44 (1999): p. 4795-4804.
28. M.J. Carmezim, A.M. Simoes, M.F. Montemor, M. Da Cunha Belo, *Corros. Sci.* 47 (2005): p. 581-591.
29. J.B. Lee, *Mater. Chem. Phys.* 99 (2006): p. 224-234.

30. M. Pourbaix, *Atlas of Electrochemical Equilibria in Aqueous Solutions,* 1st ed. (New York, NY: Pergamon Press, 1966).
31. *ASM Handbook, vol. 13, Corrosion*, 10th ed. (Materials Park, OH: ASM International, 2005).
32. M.G. Fontana, *Corrosion Engineering,* 3rd ed. (New York, NY: McGraw-Hill, 1988).
33. S. Kesavan, T.A. Mozhi, B.E. Wilde, *Corrosion* 45 (1989): p. 213-215.
34. A. Anderko, S.J. Sanders, R.D. Young, *Corrosion* 53 (1997): p. 43-53.
35. O.V. Kurov*, Corrosion* 57 (2001): p. 502-507.
36. M.J. Muñoz-Portero, J. García-Antón, J.L. Guiñón, V. Pérez-Herranz, *Corrosion* 60 (2004): p. 749-756.
37. M.J. Muñoz-Portero, J. García-Antón, J.L. Guiñón, V. Pérez-Herranz, *Corrosion* 63 (2007): p. 625-634.
38. M.J. Muñoz-Portero, J. García-Antón, J.L. Guiñón, V. Pérez-Herranz, *Corros. Sci.* 51 (2009): p. 807-819.
39. M.J. Muñoz-Portero, J. García-Antón, J.L. Guiñón, R. Leiva-García, *Corros. Sci.* 53 (2011): p. 1440-1450.
40. A.J. Bard, R. Parsons, J. Jordan, *Standard Potentials in aqueous solution,* (New York, NY: Marcel Dekker, 1985).
41. J. Rumble, *CRC Handbook of Chemistry and Physics,* 98th ed. (Boca Ratón, Florida: CRC Press, 2017).
42. B. Beverskog, I. Puigdomenech, *Corros. Sci.* 38 (1996): p. 2121-2135.
43. C.L. Kusik, H.P. Meissner, *AIChE Symp. Ser.* 74 (1978): p. 14-20.
44. H.P. Meissner*, ACS Symp. Ser.* 133 (1980): p. 495-511.
45. C.L. Kusik, H.P. Meissner, *Ind. Eng. Chem. Process Des. Dev.* 12 (1973): p. 112-115.
46. A. Anderko, R.D. Young, *Corrosion* 56 (2000): p. 543-555.
47. W. Pennington, *Refrig. Eng.* (1955): p. 57-61.
48. M.J. Muñoz-Portero, T. Nachiondo, “Development of a software application for the construction of the simplified Pourbaix diagrams used in the study of the corrosion”, 7th International Technology, Education, and Development Conference (INTED), 4-5 March (Valencia, Spain: IATED, 2013), p. 5978-5986.

FIGURE CAPTIONS

FIGURE 1. Saturated vapor pressures of aqueous LiBr solutions as a function of LiBr molality at 25 °C. The line is obtained from the thermodynamic method proposed by Meissner and Kusik and the symbols represent literature data.[46,47]

FIGURE 2. Mean activity coefficient of aqueous LiBr solutions as a function of LiBr molality at 25 °C. The line is obtained from the thermodynamic method proposed by Meissner and Kusik and the symbols represent literature data.[41]

FIGURE 3. Predominance diagram of the aqueous iron species at 25 °C.

FIGURE 4. Predominance diagram of the aqueous iron species in 400 g/L LiBr solution at 25 °C.

FIGURE 5. Predominance diagram of the aqueous iron species in 700 g/L LiBr solution at 25 °C.

FIGURE 6. Predominance diagram of the aqueous iron species in 850 g/L LiBr solution at 25 °C.

FIGURE 7. Predominance diagram of the aqueous iron species in 992 g/L LiBr solution at 25 °C.

FIGURE 8. Potential-pH diagram of iron in H_2O at 25 °C.

FIGURE 9. Potential-pH diagram of iron in aqueous 400 g/L LiBr solution at 25 °C.

FIGURE 10. Potential-pH diagram of iron in aqueous 700 g/L LiBr solution at 25 °C.

FIGURE 11. Potential-pH diagram of iron in aqueous 850 g/L LiBr solution at 25 °C.

FIGURE 12. Potential-pH diagram of iron in aqueous 992 g/L LiBr solution at 25 °C.

FIGURE 13. Simplified potential-pH diagram of iron in H_2O at 25 °C (a) in the absence and in the presence of (b) 400 g/L, (c) 700 g/L, (d) 850 g/L, and (e) 992 g/L LiBr solutions, considering a 10^{-6} activity of the aqueous iron species.

TABLE CAPTIONS

TABLE 1. Chemical species for the $Fe\text{-}Br^{-}\text{-}H_2O$ system.

TABLE 2. Electrochemical reactions not involving H^+ for the $Fe\text{-}Br^{-}\text{-}H_2O$ system.[(A)]

TABLE 3. Electrochemical reactions involving H^+ for the $Fe\text{-}Br^{-}\text{-}H_2O$ system.[(A)]

TABLE 3. Electrochemical reactions involving H^+ for the $Fe\text{-}Br^{-}\text{-}H_2O$ system (continuation 1).

TABLE 3. Electrochemical reactions involving H^+ for the $Fe\text{-}Br^{-}\text{-}H_2O$ system (continuation 2).

TABLE 3. Electrochemical reactions involving H^+ for the $Fe\text{-}Br^{-}\text{-}H_2O$ system (continuation 3).

TABLE 4. Chemical reactions involving H^+ for the $Fe\text{-}Br^{-}\text{-}H_2O$ system.[(A)]

TABLE 4. Chemical reactions involving H^+ for the $Fe\text{-}Br^{-}\text{-}H_2O$ system (continuation 1).

TABLE 4. Chemical reactions involving H^+ for the $Fe\text{-}Br^{-}\text{-}H_2O$ system (continuation 2).

TABLE 5. Chemical reactions not involving H^+ for the $Fe\text{-}Br^{-}\text{-}H_2O$ system.[(A)]

TABLE 6. Thermodynamic stability of iron species for the $Fe\text{-}Br^{-}\text{-}H_2O$ system in concentrated aqueous LiBr solutions at 25 °C.[(A)]

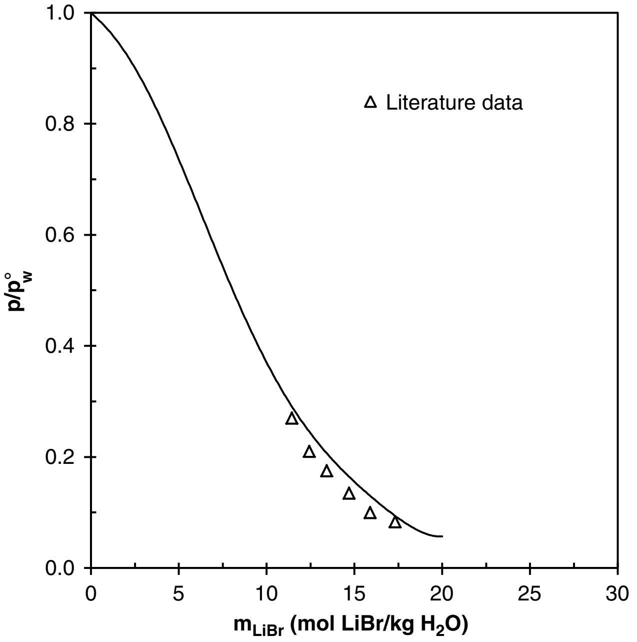

FIGURE 1.

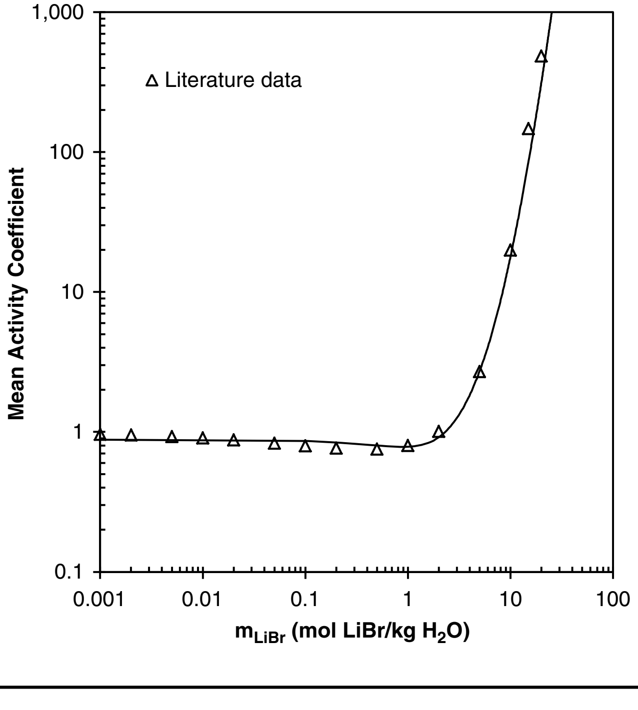

FIGURE 2.

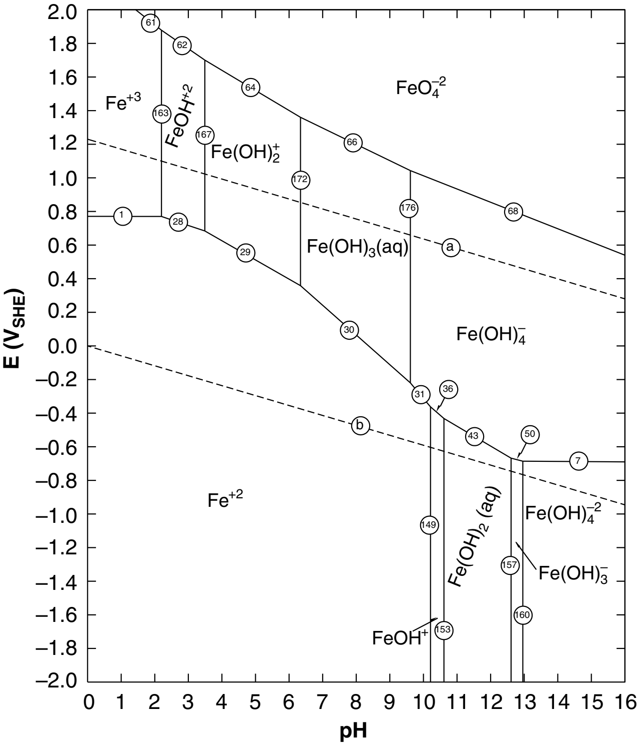

FIGURE 3.

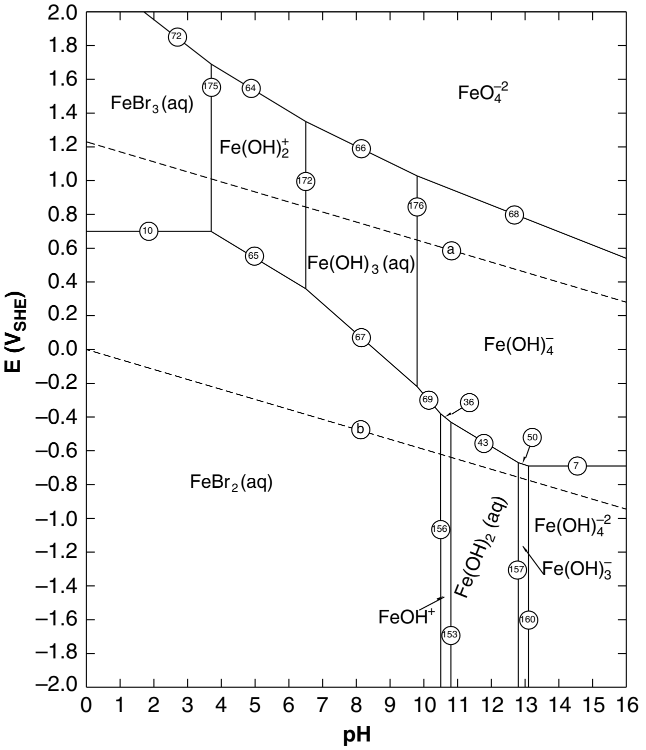

FIGURE 4.

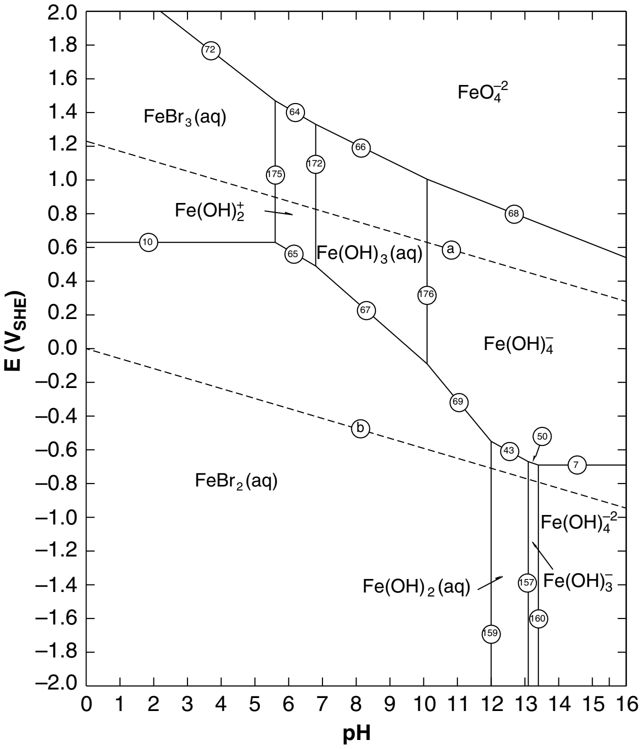

FIGURE 5.

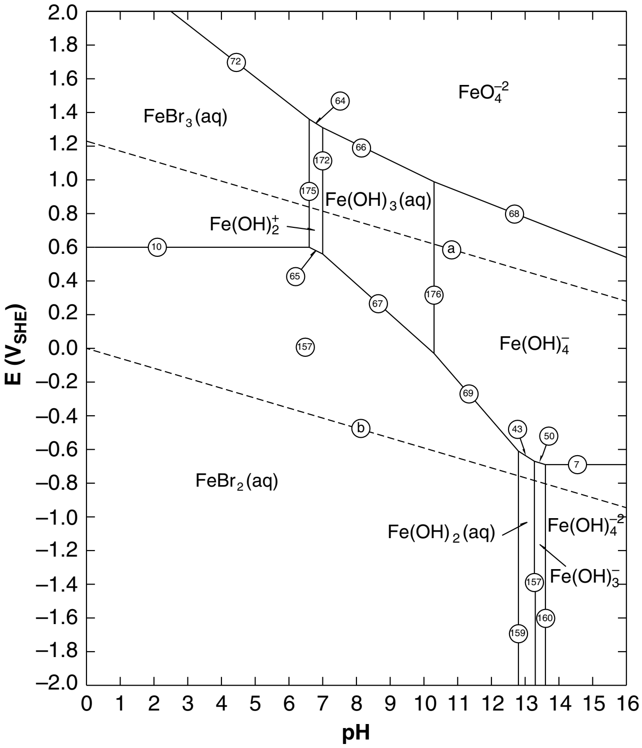

FIGURE 6.

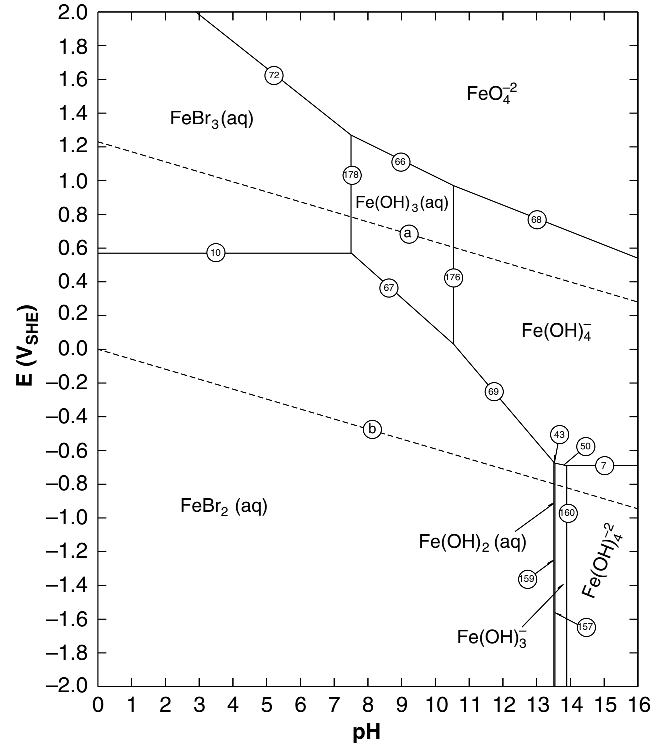

FIGURE 7.

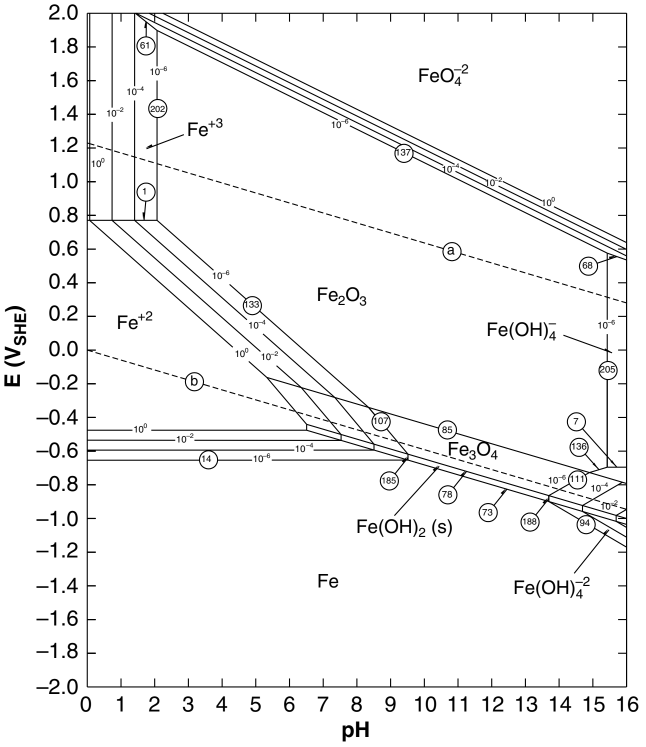

FIGURE 8.

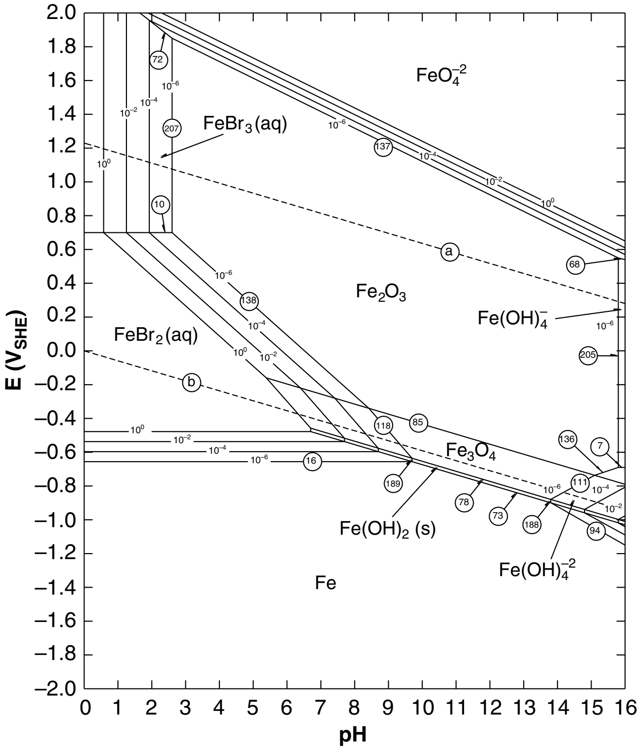

FIGURE 9.

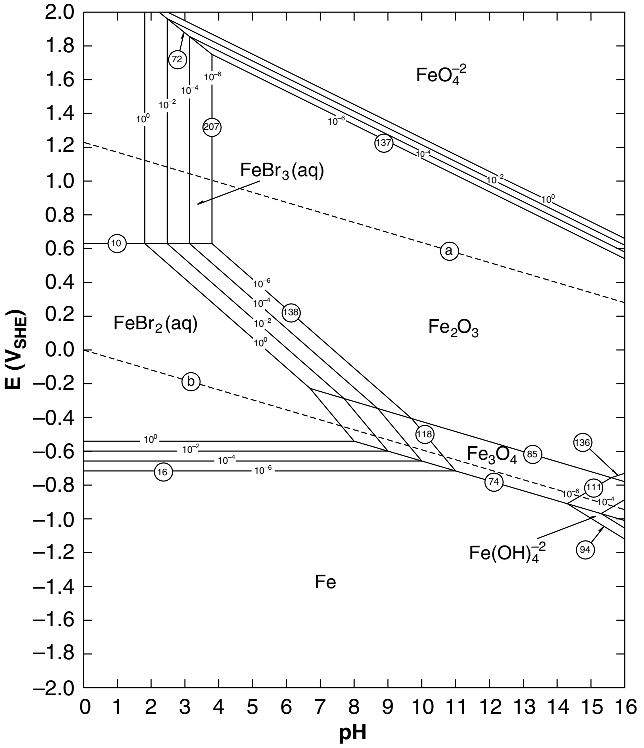

FIGURE 10.

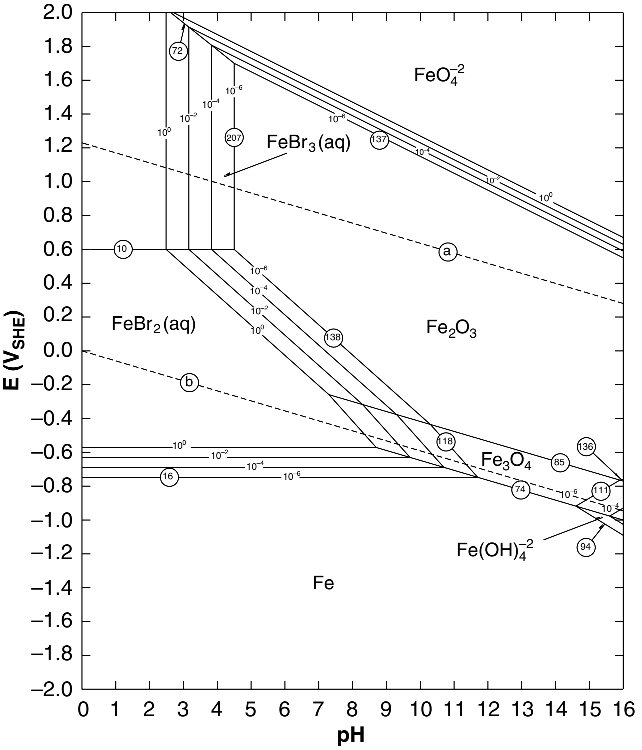

FIGURE 11.

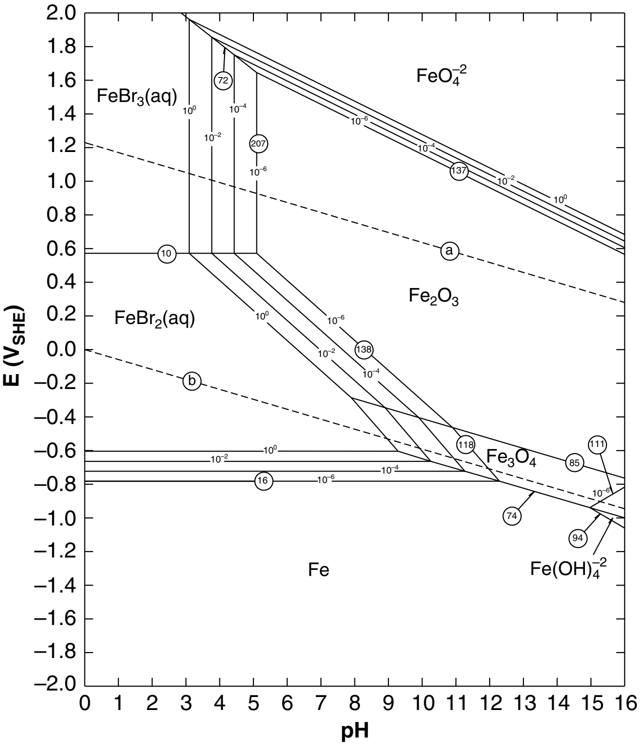

FIGURE 12.

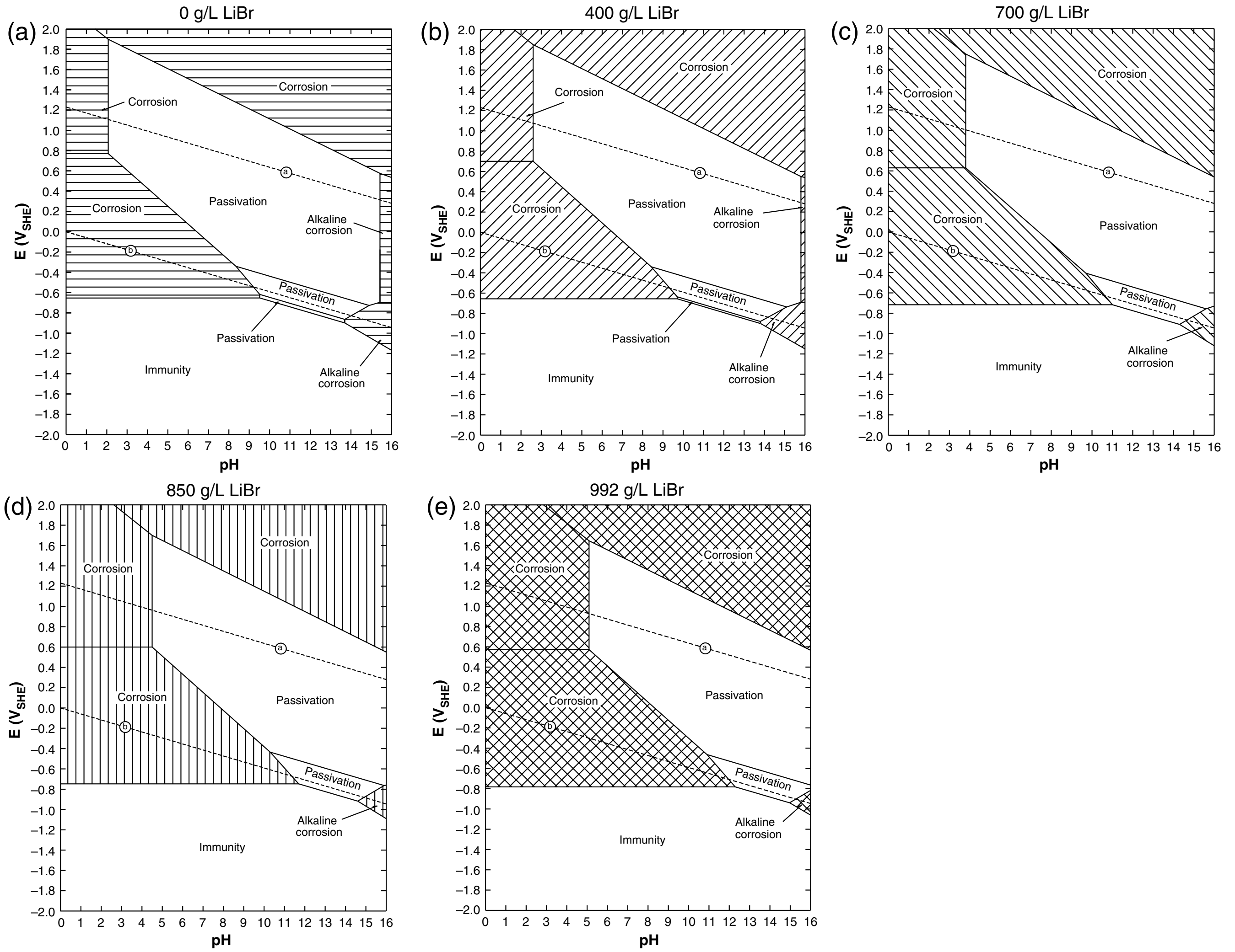
(a)
0 g/L LiBr
Corrosion
Corrosion
Corrosion
Passivation
Passivation
Passivation
Alkaline corrosion
Alkaline corrosion
Immunity
(b)
400 g/L LiBr
Corrosion
Corrosion
Corrosion
Passivation
Passivation
Passivation
Alkaline corrosion
Alkaline corrosion
Immunity
(c)
700 g/L LiBr
Corrosion
Corrosion
Corrosion
Passivation
Passivation
Alkaline corrosion
Immunity
(d)
850 g/L LiBr
Corrosion
Corrosion
Corrosion
Passivation
Passivation
Alkaline corrosion
Immunity
(e)
992 g/L LiBr
Corrosion
Corrosion
Corrosion
Passivation
Passivation
Alkaline corrosion
Immunity
a
b
E (V_{SHE})
pH
2.0 1.8 1.6 1.4 1.2 1.0 0.8 0.6 0.4 0.2 0.0 −0.2 −0.4 −0.6 −0.8 −1.0 −1.2 −1.4 −1.6 −1.8 −2.0
0 1 2 3 4 5 6 7 8 9 10 11 12 13 14 15 16

FIGURE 13.

Species	Oxidation number[A]	State[B]	$\Delta G_f°$ (kJ/mol)[C]	References
H^+		aq	0	40, 41
H_2		g	0	40, 41
O_2		g	0	40, 41
H_2O		l	– 237.178	40, 41
OH^-		aq	– 157.293	40, 41
Fe	0	s	0	42
$Fe(OH)_2(s)$	II	s	– 491.98	42
α-Fe_3O_4	II/III	s	– 1012.57	42
$Fe(OH)_3(s)$	III	s	– 705.29	42
α-FeOOH	III	s	– 485.3	42
α-Fe_2O_3	III	s	– 744.3	42
Fe^{+2}	II	aq	– 91.88	42
$FeOH^+$	II	aq	– 270.80	42
$Fe(OH)_2(aq)$	II	aq	– 447.43	42
$Fe(OH)_3^-$	II	aq	– 612.65	42
$Fe(OH)_4^{-2}$	II	aq	– 775.87	42
Fe^{+3}	III	aq	– 17.59	42
$FeOH^{+2}$	III	aq	– 242.23	42
$Fe(OH)_2^+$	III	aq	– 459.50	42
$Fe(OH)_3(aq)$	III	aq	– 660.51	42
$Fe(OH)_4^-$	III	aq	– 842.85	42
FeO_4^{-2}	VI	aq	– 322	42
Br^-		aq	– 103.97	40, 41
$FeBr_2(s)$	II	s	– 237.375	40, 41
$FeBr_3(s)$	III	s	– 242.919	40
$FeBr_2(aq)$	II	aq	– 286.81	40, 41
$FeBr^{+2}$	III	aq	– 112.1	40
$FeBr_3(aq)$	III	aq	– 316.7	40, 41

(A) Oxidation number for the iron species.

(B) aq = aqueous, g = gas, l = liquid, and s = solid.

(C) $\Delta Gf°$ = standard Gibbs free energies of formation at 25 °C.

Type	Equation	Number
Homogeneous	$Fe^{+3} + e^{-} \rightleftarrows Fe^{+2}$	1
	$FeBr^{+2} + e^{-} \rightleftarrows Fe^{+2} + Br^{-}$	2
	$FeBr_3(aq) + e^{-} \rightleftarrows Fe^{+2} + 3\,Br^{-}$	3
	$FeOH^{+2} + e^{-} \rightleftarrows FeOH^{+}$	4
	$Fe(OH)_2^{+} + e^{-} \rightleftarrows Fe(OH)_2(aq)$	5
	$Fe(OH)_3(aq) + e^{-} \rightleftarrows Fe(OH)_3^{-}$	6
	$Fe(OH)_4^{-} + e^{-} \rightleftarrows Fe(OH)_4^{-2}$	7
	$Fe^{+3} + 2\,Br^{-} + e^{-} \rightleftarrows FeBr_2(aq)$	8
	$FeBr^{+2} + Br^{-} + e^{-} \rightleftarrows FeBr_2(aq)$	9
	$FeBr_3(aq) + e^{-} \rightleftarrows FeBr_2(aq) + Br^{-}$	10
Heterogeneous with two solid species	$\mathbf{FeBr_2(s)} + 2\,e^{-} \rightleftarrows \mathbf{Fe} + 2\,Br^{-}$	11
	$\mathbf{FeBr_3(s)} + 3\,e^{-} \rightleftarrows \mathbf{Fe} + 3\,Br^{-}$	12
	$\mathbf{FeBr_3(s)} + e^{-} \rightleftarrows \mathbf{FeBr_2(s)} + Br^{-}$	13
Heterogeneous with one solid species	$Fe^{+2} + 2\,e^{-} \rightleftarrows \mathbf{Fe}$	14
	$Fe^{+3} + 3\,e^{-} \rightleftarrows \mathbf{Fe}$	15
	$FeBr_2(aq) + 2\,e^{-} \rightleftarrows \mathbf{Fe} + 2\,Br^{-}$	16
	$FeBr^{+2} + 3\,e^{-} \rightleftarrows \mathbf{Fe} + Br^{-}$	17
	$FeBr_3(aq) + 3\,e^{-} \rightleftarrows \mathbf{Fe} + 3\,Br^{-}$	18
	$Fe(OH)_2^{+} + e^{-} \rightleftarrows \mathbf{Fe(OH)_2(s)}$	19
	$\mathbf{Fe(OH)_3(s)} + e^{-} \rightleftarrows Fe(OH)_3^{-}$	20
	$\mathbf{FeOOH} + H_2O + e^{-} \rightleftarrows Fe(OH)_3^{-}$	21
	$\mathbf{Fe_2O_3} + 3\,H_2O + 2\,e^{-} \rightleftarrows 2\,Fe(OH)_3^{-}$	22
	$\mathbf{FeBr_3(s)} + e^{-} \rightleftarrows Fe^{+2} + 3\,Br^{-}$	23
	$Fe^{+3} + 2\,Br^{-} + e^{-} \rightleftarrows \mathbf{FeBr_2(s)}$	24
	$FeBr^{+2} + Br^{-} + e^{-} \rightleftarrows \mathbf{FeBr_2(s)}$	25
	$FeBr_3(aq) + e^{-} \rightleftarrows \mathbf{FeBr_2(s)} + Br^{-}$	26
	$\mathbf{FeBr_3(s)} + e^{-} \rightleftarrows FeBr_2(aq) + Br^{-}$	27

(A) Solid species are typed in bold letters. Reactions used for the construction of the potential-pH diagram for the simple Fe-H_2O system are shaded.

Type	Equation	Number
Homogeneous	$FeOH^{+2} + H^+ + e^- \rightleftarrows Fe^{+2} + H_2O$	28
	$Fe(OH)_2^+ + 2\,H^+ + e^- \rightleftarrows Fe^{+2} + 2\,H_2O$	29
	$Fe(OH)_3(aq) + 3\,H^+ + e^- \rightleftarrows Fe^{+2} + 3\,H_2O$	30
	$Fe(OH)_4^- + 4\,H^+ + e^- \rightleftarrows Fe^{+2} + 4\,H_2O$	31
	$FeO_4^{-2} + 8\,H^+ + 4\,e^- \rightleftarrows Fe^{+2} + 4\,H_2O$	32
	$Fe^{+3} + H_2O + e^- \rightleftarrows FeOH^+ + H^+$	33
	$Fe(OH)_2^+ + H^+ + e^- \rightleftarrows FeOH^+ + H_2O$	34
	$Fe(OH)_3(aq) + 2\,H^+ + e^- \rightleftarrows FeOH^+ + 2\,H_2O$	35
	$Fe(OH)_4^- + 3\,H^+ + e^- \rightleftarrows FeOH^+ + 3\,H_2O$	36
	$FeO_4^{-2} + 7\,H^+ + 4\,e^- \rightleftarrows FeOH^+ + 3\,H_2O$	37
	$FeBr^{+2} + H_2O + e^- \rightleftarrows FeOH^+ + Br^- + H^+$	38
	$FeBr_3(aq) + H_2O + e^- \rightleftarrows FeOH^+ + 3\,Br^- + H^+$	39
	$Fe^{+3} + 2\,H_2O + e^- \rightleftarrows Fe(OH)_2(aq) + 2\,H^+$	40
	$FeOH^{+2} + H_2O + e^- \rightleftarrows Fe(OH)_2(aq) + H^+$	41
	$Fe(OH)_3(aq) + H^+ + e^- \rightleftarrows Fe(OH)_2(aq) + H_2O$	42
	$Fe(OH)_4^- + 2\,H^+ + e^- \rightleftarrows Fe(OH)_2(aq) + 2\,H_2O$	43
	$FeO_4^{-2} + 6\,H^+ + 4e^- \rightleftarrows Fe(OH)_2(aq) + 2\,H_2O$	44
	$FeBr^{+2} + 2\,H_2O + e^- \rightleftarrows Fe(OH)_2(aq) + Br^- + 2\,H^+$	45
	$FeBr_3(aq) + 2\,H_2O + e^- \rightleftarrows Fe(OH)_2(aq) + 3\,Br^- + 2\,H^+$	46
	$Fe^{+3} + 3\,H_2O + e^- \rightleftarrows Fe(OH)_3^- + 3\,H^+$	47
	$FeOH^{+2} + 2\,H_2O + e^- \rightleftarrows Fe(OH)_3^- + 2\,H^+$	48
	$Fe(OH)_2^+ + H_2O + e^- \rightleftarrows Fe(OH)_3^- + H^+$	49
	$Fe(OH)_4^- + H^+ + e^- \rightleftarrows Fe(OH)_3^- + H_2O$	50
	$FeO_4^{-2} + 5\,H^+ + 4\,e^- \rightleftarrows Fe(OH)_3^- + H_2O$	51
	$FeBr^{+2} + 3\,H_2O + e^- \rightleftarrows Fe(OH)_3^- + Br^- + 3\,H^+$	52
	$FeBr_3(aq) + 3\,H_2O + e^- \rightleftarrows Fe(OH)_3^- + 3\,Br^- + 3\,H^+$	53
	$Fe^{+3} + 4\,H_2O + e^- \rightleftarrows Fe(OH)_4^{-2} + 4\,H^+$	54
	$FeOH^{+2} + 3\,H_2O + e^- \rightleftarrows Fe(OH)_4^{-2} + 3\,H^+$	55
	$Fe(OH)_2^+ + 2\,H_2O + e^- \rightleftarrows Fe(OH)_4^{-2} + 2\,H^+$	56
	$Fe(OH)_3(aq) + H_2O + e^- \rightleftarrows Fe(OH)_4^{-2} + H^+$	57
	$FeO_4^{-2} + 4\,H^+ + 4\,e^- \rightleftarrows Fe(OH)_4^{-2}$	58
	$FeBr^{+2} + 4\,H_2O + e^- \rightleftarrows Fe(OH)_4^{-2} + Br^- + 4\,H^+$	59

Type	Equation	Number
Homogeneous	$FeBr_3(aq) + 4\,H_2O + e^- \rightleftarrows Fe(OH)_4^{-2} + 3\,Br^- + 4\,H^+$	60
	$FeO_4^{-2} + 8\,H^+ + 3\,e^- \rightleftarrows Fe^{+3} + 4\,H_2O$	61
	$FeO_4^{-2} + 7\,H^+ + 3\,e^- \rightleftarrows FeOH^{+2} + 3\,H_2O$	62
	$FeOH^{+2} + 2\,Br^- + H^+ + e^- \rightleftarrows FeBr_2(aq) + H_2O$	63
	$FeO_4^{-2} + 6\,H^+ + 3\,e^- \rightleftarrows Fe(OH)_2^+ + 2\,H_2O$	64
	$Fe(OH)_2^+ + 2\,Br^- + 2\,H^+ + e^- \rightleftarrows FeBr_2(aq) + 2\,H_2O$	65
	$FeO_4^{-2} + 5\,H^+ + 3\,e^- \rightleftarrows Fe(OH)_3(aq) + H_2O$	66
	$Fe(OH)_3(aq) + 2\,Br^- + 3\,H^+ + e^- \rightleftarrows FeBr_2(aq) + 3\,H_2O$	67
	$FeO_4^{-2} + 4\,H^+ + 3\,e^- \rightleftarrows Fe(OH)_4^-$	68
	$Fe(OH)_4^- + 2\,Br^- + 4\,H^+ + e^- \rightleftarrows FeBr_2(aq) + 4\,H_2O$	69
	$FeO_4^{-2} + 2\,Br^- + 8\,H^+ + 4\,e^- \rightleftarrows FeBr_2(aq) + 4\,H_2O$	70
	$FeO_4^{-2} + Br^- + 8\,H^+ + 3\,e^- \rightleftarrows FeBr^{+2} + 4\,H_2O$	71
	$FeO_4^{-2} + 3\,Br^- + 8\,H^+ + 3\,e^- \rightleftarrows FeBr_3(aq) + 4\,H_2O$	72
Heterogeneous with two solid species	$\mathbf{Fe(OH)_2(s)} + 2\,H^+ + 2\,e^- \rightleftarrows \mathbf{Fe} + 2\,H_2O$	73
	$\mathbf{Fe_3O_4} + 8\,H^+ + 8\,e^- \rightleftarrows 3\,\mathbf{Fe} + 4\,H_2O$	74
	$\mathbf{Fe(OH)_3(s)} + 3\,H^+ + 3\,e^- \rightleftarrows \mathbf{Fe} + 3\,H_2O$	75
	$\mathbf{FeOOH} + 3\,H^+ + 3\,e^- \rightleftarrows \mathbf{Fe} + 2\,H_2O$	76
	$\mathbf{Fe_2O_3} + 6\,H^+ + 6\,e^- \rightleftarrows 2\,\mathbf{Fe} + 3\,H_2O$	77
	$\mathbf{Fe_3O_4} + 2\,H^+ + 2\,H_2O + 2\,e^- \rightleftarrows 3\,\mathbf{Fe(OH)_2(s)}$	78
	$\mathbf{Fe(OH)_3(s)} + H^+ + e^- \rightleftarrows \mathbf{Fe(OH)_2(s)} + H_2O$	79
	$\mathbf{FeOOH} + H^+ + e^- \rightleftarrows \mathbf{Fe(OH)_2(s)}$	80
	$\mathbf{Fe_2O_3} + 2\,H^+ + H_2O + 2e^- \rightleftarrows 2\,\mathbf{Fe(OH)_2(s)}$	81
	$\mathbf{FeBr_3(s)} + 2\,H_2O + e^- \rightleftarrows \mathbf{Fe(OH)_2(s)} + 3\,Br^- + 2\,H^+$	82
	$3\,\mathbf{Fe(OH)_3(s)} + H^+ + e^- \rightleftarrows \mathbf{Fe_3O_4} + 5\,H_2O$	83
	$3\,\mathbf{FeOOH} + H^+ + e^- \rightleftarrows \mathbf{Fe_3O_4} + 2\,H_2O$	84
	$3\,\mathbf{Fe_2O_3} + 2\,H^+ + 2e^- \rightleftarrows 2\,\mathbf{Fe_3O_4} + H_2O$	85
	$\mathbf{Fe_3O_4} + 6\,Br^- + 8\,H^+ + 2\,e^- \rightleftarrows 3\,\mathbf{FeBr_2(s)} + 4\,H_2O$	86
	$3\,\mathbf{FeBr_3(s)} + 4\,H_2O + e^- \rightleftarrows \mathbf{Fe_3O_4} + 9\,Br^- + 8\,H^+$	87
	$\mathbf{Fe(OH)_3(s)} + 2\,Br^- + 3\,H^+ + e^- \rightleftarrows \mathbf{FeBr_2(s)} + 3\,H_2O$	88
	$\mathbf{FeOOH} + 2\,Br^- + 3\,H^+ + e^- \rightleftarrows \mathbf{FeBr_2(s)} + 2\,H_2O$	89
	$\mathbf{Fe_2O_3} + 4\,Br^- + 6\,H^+ + 2\,e^- \rightleftarrows 2\,\mathbf{FeBr_2(s)} + 3\,H_2O$	90

Type	Equation	Number
Heterogeneous with one solid species	$FeOH^+ + H^+ + 2\,e^- \rightleftarrows \mathbf{Fe} + H_2O$	91
	$Fe(OH)_2(aq) + 2\,H^+ + 2\,e^- \rightleftarrows \mathbf{Fe} + 2\,H_2O$	92
	$Fe(OH)_3^- + 3\,H^+ + 2\,e^- \rightleftarrows \mathbf{Fe} + 3\,H_2O$	93
	$Fe(OH)_4^{-2} + 4\,H^+ + 2\,e^- \rightleftarrows \mathbf{Fe} + 4\,H_2O$	94
	$FeOH^{+2} + H^+ + 3\,e^- \rightleftarrows \mathbf{Fe} + H_2O$	95
	$Fe(OH)_2^+ + 2\,H^+ + 3\,e^- \rightleftarrows \mathbf{Fe} + 2\,H_2O$	96
	$Fe(OH)_3(aq) + 3\,H^+ + 3\,e^- \rightleftarrows \mathbf{Fe} + 3\,H_2O$	97
	$Fe(OH)_4^- + 4\,H^+ + 3\,e^- \rightleftarrows \mathbf{Fe} + 4\,H_2O$	98
	$FeO_4^{-2} + 8\,H^+ + 6\,e^- \rightleftarrows \mathbf{Fe} + 4\,H_2O$	99
	$Fe^{+3} + 2\,H_2O + e^- \rightleftarrows \mathbf{Fe(OH)_2(s)} + 2\,H^+$	100
	$FeOH^{+2} + H_2O + e^- \rightleftarrows \mathbf{Fe(OH)_2(s)} + H^+$	101
	$Fe(OH)_3(aq) + H^+ + e^- \rightleftarrows \mathbf{Fe(OH)_2(s)} + H_2O$	102
	$Fe(OH)_4^- + 2\,H^+ + e^- \rightleftarrows \mathbf{Fe(OH)_2(s)} + 2\,H_2O$	103
	$FeO_4^{-2} + 6\,H^+ + 4\,e^- \rightleftarrows \mathbf{Fe(OH)_2(s)} + 2\,H_2O$	104
	$FeBr^{+2} + 2\,H_2O + e^- \rightleftarrows \mathbf{Fe(OH)_2(s)} + Br^- + 2\,H^+$	105
	$FeBr_3(aq) + 2\,H_2O + e^- \rightleftarrows \mathbf{Fe(OH)_2(s)} + 3\,Br^- + 2\,H^+$	106
	$\mathbf{Fe_3O_4} + 8\,H^+ + 2\,e^- \rightleftarrows 3\,Fe^{+2} + 4\,H_2O$	107
	$\mathbf{Fe_3O_4} + 5\,H^+ + 2\,e^- \rightleftarrows 3\,FeOH^+ + H_2O$	108
	$\mathbf{Fe_3O_4} + 2\,H^+ + 2\,H_2O + 2\,e^- \rightleftarrows 3\,Fe(OH)_2(aq)$	109
	$\mathbf{Fe_3O_4} + 5\,H_2O + 2\,e^- \rightleftarrows 3\,Fe(OH)_3^- + H^+$	110
	$\mathbf{Fe_3O_4} + 8\,H_2O + 2\,e^- \rightleftarrows 3\,Fe(OH)_4^{-2} + 4\,H^+$	111
	$3\,Fe^{+3} + 4\,H_2O + e^- \rightleftarrows \mathbf{Fe_3O_4} + 8\,H^+$	112
	$3\,FeOH^{+2} + H_2O + e^- \rightleftarrows \mathbf{Fe_3O_4} + 5\,H^+$	113
	$3\,Fe(OH)_2^+ + e^- \rightleftarrows \mathbf{Fe_3O_4} + 2\,H^+ + 2\,H_2O$	114
	$3\,Fe(OH)_3(aq) + H^+ + e^- \rightleftarrows \mathbf{Fe_3O_4} + 5\,H_2O$	115
	$3\,Fe(OH)_4^- + 4\,H^+ + e^- \rightleftarrows \mathbf{Fe_3O_4} + 8\,H_2O$	116
	$3\,FeO_4^{-2} + 16\,H^+ + 10\,e^- \rightleftarrows \mathbf{Fe_3O_4} + 8\,H_2O$	117
	$\mathbf{Fe_3O_4} + 6\,Br^- + 8\,H^+ + 2e^- \rightleftarrows 3\,FeBr_2(aq) + 4\,H_2O$	118
	$3\,FeBr^{+2} + 4\,H_2O + e^- \rightleftarrows \mathbf{Fe_3O_4} + 3\,Br^- + 8\,H^+$	119
	$3\,FeBr_3(aq) + 4\,H_2O + e^- \rightleftarrows \mathbf{Fe_3O_4} + 9\,Br^- + 8\,H^+$	120
	$\mathbf{Fe(OH)_3(s)} + 3\,H^+ + e^- \rightleftarrows Fe^{+2} + 3\,H_2O$	121
	$\mathbf{Fe(OH)_3(s)} + 2\,H^+ + e^- \rightleftarrows FeOH^+ + 2\,H_2O$	122

Type	Equation	Number
Heterogeneous with one solid species	$\mathbf{Fe(OH)_3(s)} + H^+ + e^- \rightleftarrows Fe(OH)_2(aq) + H_2O$	123
	$\mathbf{Fe(OH)_3(s)} + H_2O + e^- \rightleftarrows Fe(OH)_4^{-2} + H^+$	124
	$FeO_4^{-2} + 5\,H^+ + 3\,e^- \rightleftarrows \mathbf{Fe(OH)_3(s)} + H_2O$	125
	$\mathbf{Fe(OH)_3(s)} + 2\,Br^- + 3\,H^+ + e^- \rightleftarrows FeBr_2\,(aq) + 3\,H_2O$	126
	$\mathbf{FeOOH} + 3\,H^+ + e^- \rightleftarrows Fe^{+2} + 2\,H_2O$	127
	$\mathbf{FeOOH} + 2\,H^+ + e^- \rightleftarrows FeOH^+ + H_2O$	128
	$\mathbf{FeOOH} + H^+ + e^- \rightleftarrows Fe(OH)_2(aq)$	129
	$\mathbf{FeOOH} + 2\,H_2O + e^- \rightleftarrows Fe(OH)_4^{-2} + H^+$	130
	$FeO_4^{-2} + 5\,H^+ + 3\,e^- \rightleftarrows \mathbf{FeOOH} + 2\,H_2O$	131
	$\mathbf{FeOOH} + 2\,Br^- + 3\,H^+ + e^- \rightleftarrows FeBr_2(aq) + 2\,H_2O$	132
	$\mathbf{Fe_2O_3} + 6\,H^+ + 2\,e^- \rightleftarrows 2\,Fe^{+2} + 3\,H_2O$	133
	$\mathbf{Fe_2O_3} + 4\,H^+ + 2\,e^- \rightleftarrows 2\,FeOH^+ + H_2O$	134
	$\mathbf{Fe_2O_3} + 2\,H^+ + H_2O + 2\,e^- \rightleftarrows 2\,Fe(OH)_2(aq)$	135
	$\mathbf{Fe_2O_3} + 5\,H_2O + 2\,e^- \rightleftarrows 2\,Fe(OH)_4^{-2} + 2\,H^+$	136
	$2\,FeO_4^{-2} + 10\,H^+ + 6\,e^- \rightleftarrows \mathbf{Fe_2O_3} + 5\,H_2O$	137
	$\mathbf{Fe_2O_3} + 4\,Br^- + 6\,H^+ + 2\,e^- \rightleftarrows 2\,FeBr_2(aq) + 3\,H_2O$	138
	$\mathbf{FeBr_3(s)} + H_2O + e^- \rightleftarrows FeOH^+ + 3\,Br^- + H^+$	139
	$\mathbf{FeBr_3(s)} + 2\,H_2O + e^- \rightleftarrows Fe(OH)_2(aq) + 3\,Br^- + 2\,H^+$	140
	$\mathbf{FeBr_3(s)} + 3\,H_2O + e^- \rightleftarrows Fe(OH)_3^- + 3\,Br^- + 3\,H^+$	141
	$\mathbf{FeBr_3(s)} + 4\,H_2O + e^- \rightleftarrows Fe(OH)_4^{-2} + 3\,Br^- + 4\,H^+$	142
	$FeOH^{+2} + 2\,Br^- + H^+ + e^- \rightleftarrows \mathbf{FeBr_2(s)} + H_2O$	143
	$Fe(OH)_2^+ + 2\,Br^- + 2\,H^+ + e^- \rightleftarrows \mathbf{FeBr_2(s)} + 2\,H_2O$	144
	$Fe(OH)_3(aq) + 2\,Br^- + 3\,H^+ + e^- \rightleftarrows \mathbf{FeBr_2(s)} + 3\,H_2O$	145
	$Fe(OH)_4^- + 2\,Br^- + 4\,H^+ + e^- \rightleftarrows \mathbf{FeBr_2(s)} + 4\,H_2O$	146
	$FeO_4^{-2} + 2\,Br^- + 8\,H^+ + 4\,e^- \rightleftarrows \mathbf{FeBr_2(s)} + 4\,H_2O$	147
	$FeO_4^{-2} + 3\,Br^- + 8\,H^+ + 3\,e^- \rightleftarrows \mathbf{FeBr_3(s)} + 4\,H_2O$	148

(A) Solid species are typed in bold letters. Reactions used for the construction of the potential-pH diagram for the simple Fe-H_2O system are shaded.

Type	Equation	Number
Homogeneous	$Fe^{+2} + H_2O \rightleftarrows FeOH^+ + H^+$	149
	$Fe^{+2} + 2\,H_2O \rightleftarrows Fe(OH)_2(aq) + 2\,H^+$	150
	$Fe^{+2} + 3\,H_2O \rightleftarrows Fe(OH)_3^- + 3\,H^+$	151
	$Fe^{+2} + 4\,H_2O \rightleftarrows Fe(OH)_4^{-2} + 4\,H^+$	152
	$FeOH^+ + H_2O \rightleftarrows Fe(OH)_2(aq) + H^+$	153
	$FeOH^+ + 2\,H_2O \rightleftarrows Fe(OH)_3^- + 2\,H^+$	154
	$FeOH^+ + 3\,H_2O \rightleftarrows Fe(OH)_4^{-2} + 3\,H^+$	155
	$FeBr_2(aq) + H_2O \rightleftarrows FeOH^+ + 2\,Br^- + H^+$	156
	$Fe(OH)_2(aq) + H_2O \rightleftarrows Fe(OH)_3^- + H^+$	157
	$Fe(OH)_2(aq) + 2\,H_2O \rightleftarrows Fe(OH)_4^{-2} + 2\,H^+$	158
	$FeBr_2(aq) + 2\,H_2O \rightleftarrows Fe(OH)_2(aq) + 2\,Br^- + 2\,H^+$	159
	$Fe(OH)_3^- + H_2O \rightleftarrows Fe(OH)_4^{-2} + H^+$	160
	$FeBr_2(aq) + 3\,H_2O \rightleftarrows Fe(OH)_3^- + 2\,Br^- + 3\,H^+$	161
	$FeBr_2(aq) + 4\,H_2O \rightleftarrows Fe(OH)_4^{-2} + 2\,Br^- + 4\,H^+$	162
	$Fe^{+3} + H_2O \rightleftarrows FeOH^{+2} + H^+$	163
	$Fe^{+3} + 2\,H_2O \rightleftarrows Fe(OH)_2^+ + 2\,H^+$	164
	$Fe^{+3} + 3\,H_2O \rightleftarrows Fe(OH)_3(aq) + 3\,H^+$	165
	$Fe^{+3} + 4\,H_2O \rightleftarrows Fe(OH)_4^- + 4\,H^+$	166
	$FeOH^{+2} + H_2O \rightleftarrows Fe(OH)_2^+ + H^+$	167
	$FeOH^{+2} + 2\,H_2O \rightleftarrows Fe(OH)_3(aq) + 2\,H^+$	168
	$FeOH^{+2} + 3\,H_2O \rightleftarrows Fe(OH)_4^- + 3\,H^+$	169
	$FeBr^{+2} + H_2O \rightleftarrows FeOH^{+2} + Br^- + H^+$	170
	$FeBr_3(aq) + H_2O \rightleftarrows FeOH^{+2} + 3\,Br^- + H^+$	171
	$Fe(OH)_2^+ + H_2O \rightleftarrows Fe(OH)_3(aq) + H^+$	172
	$Fe(OH)_2^+ + 2\,H_2O \rightleftarrows Fe(OH)_4^- + 2\,H^+$	173
	$FeBr^{+2} + 2\,H_2O \rightleftarrows Fe(OH)_2^+ + Br^- + 2\,H^+$	174
	$FeBr_3(aq) + 2\,H_2O \rightleftarrows Fe(OH)_2^+ + 3\,Br^- + 2\,H^+$	175
	$Fe(OH)_3(aq) + H_2O \rightleftarrows Fe(OH)_4^- + H^+$	176
	$FeBr^{+2} + 3\,H_2O \rightleftarrows Fe(OH)_3(aq) + Br^- + 3\,H^+$	177
	$FeBr_3(aq) + 3\,H_2O \rightleftarrows Fe(OH)_3(aq) + 3\,Br^- + 3\,H^+$	178
	$FeBr^{+2} + 4\,H_2O \rightleftarrows Fe(OH)_4^- + Br^- + 4\,H^+$	179
	$FeBr_3(aq) + 4\,H_2O \rightleftarrows Fe(OH)_4^- + 3\,Br^- + 4\,H^+$	180

Type	Equation	Number
Heterogeneous with two solid species	$\mathbf{FeBr_2(s)} + 2\,H_2O \rightleftarrows \mathbf{Fe(OH)_2(s)} + 2\,Br^- + 2\,H^+$	181
	$\mathbf{FeBr_3(s)} + 3\,H_2O \rightleftarrows \mathbf{Fe(OH)_3(s)} + 3\,Br^- + 3\,H^+$	182
	$\mathbf{FeBr_3(s)} + 2\,H_2O \rightleftarrows \mathbf{FeOOH} + 3\,Br^- + 3\,H^+$	183
	$2\,\mathbf{FeBr_3(s)} + 3\,H_2O \rightleftarrows \mathbf{Fe_2O_3} + 6\,Br^- + 6\,H^+$	184
Heterogeneous with one solid species	$Fe^{+2} + 2\,H_2O \rightleftarrows \mathbf{Fe(OH)_2(s)} + 2\,H^+$	185
	$FeOH^+ + H_2O \rightleftarrows \mathbf{Fe(OH)_2(s)} + H^+$	186
	$\mathbf{Fe(OH)_2(s)} + H_2O \rightleftarrows Fe(OH)_3^- + H^+$	187
	$\mathbf{Fe(OH)_2(s)} + 2\,H_2O \rightleftarrows Fe(OH)_4^{-2} + 2\,H^+$	188
	$FeBr_2(aq) + 2\,H_2O \rightleftarrows \mathbf{Fe(OH)_2(s)} + 2\,Br^- + 2\,H^+$	189
	$Fe^{+3} + 3\,H_2O \rightleftarrows \mathbf{Fe(OH)_3(s)} + 3\,H^+$	190
	$FeOH^{+2} + 2\,H_2O \rightleftarrows \mathbf{Fe(OH)_3(s)} + 2\,H^+$	191
	$Fe(OH)_2^+ + H_2O \rightleftarrows \mathbf{Fe(OH)_3(s)} + H^+$	192
	$\mathbf{Fe(OH)_3(s)} + H_2O \rightleftarrows Fe(OH)_4^- + H^+$	193
	$FeBr^{+2} + 3\,H_2O \rightleftarrows \mathbf{Fe(OH)_3(s)} + Br^- + 3\,H^+$	194
	$FeBr_3(aq) + 3\,H_2O \rightleftarrows \mathbf{Fe(OH)_3(s)} + 3\,Br^- + 3\,H^+$	195
	$Fe^{+3} + 2\,H_2O \rightleftarrows \mathbf{FeOOH} + 3\,H^+$	196
	$FeOH^{+2} + H_2O \rightleftarrows \mathbf{FeOOH} + 2\,H^+$	197
	$Fe(OH)_2^+ \rightleftarrows \mathbf{FeOOH} + H^+$	198
	$\mathbf{FeOOH} + 2\,H_2O \rightleftarrows Fe(OH)_4^- + H^+$	199
	$FeBr^{+2} + 2\,H_2O \rightleftarrows \mathbf{FeOOH} + Br^- + 3\,H^+$	200
	$FeBr_3(aq) + 2\,H_2O \rightleftarrows \mathbf{FeOOH} + 3\,Br^- + 3\,H^+$	201
	$2\,Fe^{+3} + 3\,H_2O \rightleftarrows \mathbf{Fe_2O_3} + 6\,H^+$	202
	$2\,FeOH^{+2} + H_2O \rightleftarrows \mathbf{Fe_2O_3} + 4\,H^+$	203
	$2\,Fe(OH)_2^+ \rightleftarrows \mathbf{Fe_2O_3} + 2\,H^+ + H_2O$	204
	$\mathbf{Fe_2O_3} + 5\,H_2O \rightleftarrows 2\,Fe(OH)_4^- + 2\,H^+$	205
	$2\,FeBr^{+2} + 3\,H_2O \rightleftarrows \mathbf{Fe_2O_3} + 2\,Br^- + 6\,H^+$	206
	$2\,FeBr_3(aq) + 3\,H_2O \rightleftarrows \mathbf{Fe_2O_3} + 6\,Br^- + 6\,H^+$	207
	$\mathbf{FeBr_2(s)} + H_2O \rightleftarrows FeOH^+ + 2\,Br^- + H^+$	208
	$\mathbf{FeBr_2(s)} + 2\,H_2O \rightleftarrows Fe(OH)_2(aq) + 2\,Br^- + 2\,H^+$	209
	$\mathbf{FeBr_2(s)} + 3\,H_2O \rightleftarrows Fe(OH)_3^- + 2\,Br^- + 3\,H^+$	210
	$\mathbf{FeBr_2(s)} + 4\,H_2O \rightleftarrows Fe(OH)_4^{-2} + 2\,Br^- + 4\,H^+$	211

Type	Equation	Number
Heterogeneous with one solid species	$\mathbf{FeBr_3(s)} + H_2O \rightleftarrows FeOH^{+2} + 3\,Br^- + H^+$	212
	$\mathbf{FeBr_3(s)} + 2\,H_2O \rightleftarrows Fe(OH)_2^+ + 3\,Br^- + 2\,H^+$	213
	$\mathbf{FeBr_3(s)} + 3\,H_2O \rightleftarrows Fe(OH)_3(aq) + 3\,Br^- + 3\,H^+$	214
	$\mathbf{FeBr_3(s)} + 4\,H_2O \rightleftarrows Fe(OH)_4^- + 3\,Br^- + 4\,H^+$	215

(A) Solid species are typed in bold letters. Reactions used for the construction of the potential-pH diagram for the simple Fe-H_2O system are shaded.

Type	Equation	Number
Homogeneous	$Fe^{+2} + 2\,Br^{-} \rightleftarrows FeBr_2(aq)$	216
	$Fe^{+3} + Br^{-} \rightleftarrows FeBr^{+2}$	217
	$Fe^{+3} + 3\,Br^{-} \rightleftarrows FeBr_3(aq)$	218
	$FeBr^{+2} + 2\,Br^{-} \rightleftarrows FeBr_3(aq)$	219
Heterogeneous with two solid species	$\mathbf{Fe(OH)_3(s)} \rightleftarrows \mathbf{FeOOH} + H_2O$	220
	$2\,\mathbf{Fe(OH)_3(s)} \rightleftarrows \mathbf{Fe_2O_3} + 3\,H_2O$	221
	$2\,\mathbf{FeOOH} \rightleftarrows \mathbf{Fe_2O_3} + H_2O$	222
Heterogeneous with one solid species	$\mathbf{Fe(OH)_2(s)} \rightleftarrows Fe(OH)_2(aq)$	223
	$\mathbf{Fe(OH)_3(s)} \rightleftarrows Fe(OH)_3(aq)$	224
	$\mathbf{FeOOH} + H_2O \rightleftarrows Fe(OH)_3(aq)$	225
	$\mathbf{Fe_2O_3} + 3\,H_2O \rightleftarrows 2\,Fe(OH)_3(aq)$	226
	$Fe^{+2} + 2\,Br^{-} \rightleftarrows \mathbf{FeBr_2(s)}$	227
	$Fe^{+3} + 3\,Br^{-} \rightleftarrows \mathbf{FeBr_3(s)}$	228
	$\mathbf{FeBr_2(s)} \rightleftarrows FeBr_2(aq)$	229
	$\mathbf{FeBr_3(s)} \rightleftarrows FeBr^{+2} + 2\,Br^{-}$	230
	$\mathbf{FeBr_3(s)} \rightleftarrows FeBr_3\,(aq)$	231

(A) Solid species are typed in bold letters. Reactions used for the construction of the potential-pH diagram for the simple Fe-H_2O system are shaded.

Species	[LiBr] = 0 g/L $(Br^-) = 0$ $(H_2O) = 1$	[LiBr] = 400 g/L $(Br^-) = 15.61$ $(H_2O) = 0.715$	[LiBr] = 700 g/L $(Br^-) = 194.77$ $(H_2O) = 0.358$	[LiBr] = 850 g/L $(Br^-) = 650.06$ $(H_2O) = 0.216$	[LiBr] = 992 g/L $(Br^-) = 2,042.65$ $(H_2O) = 0.118$
Fe	b	b	b	b	b
$Fe(OH)_2(s)$	b	b			
α-Fe_3O_4	b	b	b	b	b
$Fe(OH)_3(s)$					
α-FeOOH					
α-Fe_2O_3	b	b	b	b	b
Fe^{+2}	a b				
$FeOH^+$	a	a			
$Fe(OH)_2(aq)$	a	a	a	a	a
$Fe(OH)_3^-$	a	a	a	a	a
$Fe(OH)_4^{-2}$	a b	a b	a b	a b	a b
Fe^{+3}	a b				
$FeOH^{+2}$	a				
$Fe(OH)_2^+$	a	a	a	a	
$Fe(OH)_3(aq)$	a	a	a	a	a
$Fe(OH)_4^-$	a b	a b	a	a	a
FeO_4^{-2}	a b	a b	a b	a b	a b
$FeBr_2(s)$					
$FeBr_3(s)$					
$FeBr_2(aq)$		a b	a b	a b	a b
$FeBr^{+2}$					
$FeBr_3(aq)$		a b	a b	a b	a b

(A) a = it appears in the predominance diagram of the aqueous iron species, b = it appears in the potential-pH diagram of iron.